Arabian Journal of Chemistry (2020) 13, 6510–6522

King Saud University

Arabian Journal of Chemistry

www.ksu.edu.sa
www.sciencedirect.com

ORIGINAL ARTICLE

Utilization of olive pomace in nano MgO modification for sorption of Ni(II) and Cu(II) metal ions from aqueous solutions

G.A. Dakroury [a,*], Sh.F. Abo-Zahra [a], H.S. Hassan [b]

[a] Nuclear Chemistry Department, Hot Laboratories Centre, Atomic Energy Authority, P.O. 13759, Cairo, Egypt
[b] Waste Management Department, Hot Laboratories Centre, Atomic Energy Authority, P.O. 13759, Cairo, Egypt

Received 7 March 2020; accepted 3 June 2020
Available online 18 June 2020

KEYWORDS

Nano magnesium oxide;
Olive pomace;
Sorption;
Heavy metals

Abstract Magnesium oxide nanoparticles were synthesized and modified by olive pomace (NMOOP700) as a novel sorbent and characterized using Fourier Transform Infrared Spectra, Scanning Electron Microscope, Transmission Electron Microscope, X-ray Diffraction, Differential Thermal Analysis and Thermal Gravimetric Analysis. Sorption of Cu (II) or Ni (II) ions were achieved taking into account important parameters including initial pH of the medium, contact time, initial metal ion concentration and temperature. A comparative study between Magnesium oxide nanoparticles and NMOOP700 material for the sorption of Cu (II) or Ni (II) ions was implemented. The obtained data revealed that the sorption process is significantly improved using NMOOP700. The monolayer capacity of Ni (II) and Cu (II) metal ions on NMOOP700 at pH 5 were found to be 149.93 ± 4.4 and 186.219 ± 6.3 mg/g, respectively. Findings of the present work highlight the potential use of NMOOP700 as a novel and effective sorbent material for the removal of Cu (II) or Ni (II) ions from the liquid phase.

1. Introduction

Industrial waste has become one of the most important problems facing industrial advanced countries to maintain environmental safety. There are several methods to treat the metal- contaminated effluent such as precipitation (González-Muñozet al., 2006; Matlock et al., 2002), ion exchange (Swamy et al., 2011; Kang et al., 2004; Alyüz and Veli, 2009; Caetano et al., 2009) coagulation/electrocoagulation or membrane filtration (Labanda et al., 2009; Landaburu-Aguirre et al., 2009; Landaburu-Aguirr et al., 2010; Acero et al., 2005) and adsorption (Al-Jlil and Alsewailem, 2009; Hima et al., 2007; Kour et al. 2013; Yan et al., 2013), etc. Waste water treatment selection methods are based on the concentration of waste and the cost of treatment. Adsorption is one of the most efficient treatment processes that can replace other more expensive water treatment methods (Thanh et al., 2012; Mohan and Pittman, 2007). A number of inorganic and organic adsorbents have been suggested for use in adsorption methods such as laterite iron concretion, clays, activated carbon, biomasses, and

* Corresponding author.
E-mail address: gigidakrory@gmail.com (G.A. Dakroury).
Peer review under responsibility of King Saud University.

Production and hosting by Elsevier

https://doi.org/10.1016/j.arabjc.2020.06.008
1878-5352 © 2020 Published by Elsevier B.V. on behalf of King Saud University.

zeolites, are being used as adsorbents for the treatment of polluted water with heavy metal (Mohan and Pittman, 2007; Vieira et al., 2010; Garg et al., 2008; Van Dang et al 2008).

Recently, metal oxides have been used as sorbents to dispose industrial waste such as iron oxide (Van Benschoten et al., 1994; Raven et al., 1998; Dixit and Hering, 2003), aluminium oxide (Caston et al., 1995; Lin and Wu, 2001; Patra et al., 2012), titanium oxide (Pena et al., 2005; Jegadeesan et al., 2010; Xu et al., 2010), manganese oxide (Lenoble et al., 2004; Agrawal et al., 2006; Lafferty et al., 2010), zirconium oxide (Hristovski et al., 2008; Hang et al., 2012).

The nano-sized metal oxides are classified as promising ones for heavy metals removal from aqueous systems (Hua et al., 2012). This is because of their large surface areas and high activities caused by the size quantization effect (Henglein, 1989; El-Sayed, 2001).

Magnesium oxide (MgO) is one of the promising adsorbents because it is abundant, non-toxic, chemical, thermal and radiation stabilities (Abdullah et al., 2016), and environmentally friendly material with high specific surface area and easy regeneration (Vu et al., 2014). The adsorption properties of MgO can be further enhanced by the synergetic effects of electrostatic interaction and inner-sphere complex formation that could be introduced by specific chemical modifications. The MgO/chitosan composite prepared by a chemical precipitation method was used for adsorption of methyl orange and antibacterial (Haldorai and Shim, 2014).

Olive pomace, the residual of production of olive oil, contains essentially Hemicelluloses, cellulose, and lignin (Demirbas, 2004). By its organic nature, olive pomace can serve as a pore-forming agent i.e. it became a modifier for some adsorbents. In fact, during the sintering process, the combustion of olive pomace would generate pores. Further, the ashes produced in the combustion could become part of the ceramic matrix, due to the formation of vitreous phase during the sintering process.

Our study aimed to prepare nano magnesium oxide by sol-gel technique and use a 25% olive pomace to improve it. Olive pomace vaporized at the calcination temperature of 700 °C and leaves a porous structure. Different analytical techniques used to characterize the samples as FTIR, SEM, TEM, and XRD, Particle size analyzer, BET, TGA/DTA, and pore size distribution. The calcined modified powder used as a sorbent for some heavy metals from aqueous solution such as Cu (II) and Ni (II). The physicochemical parameters involved during this adsorption investigated. The study of some kinetic and isothermal models and the thermodynamic nature of the sorption reaction studied.

2. Experimental

2.1. Chemical reagents

All the reagents used in this study were analytical grade (AR Grade) and used as received without further purification. $MgCl_2{\cdot}6H_2O$ purchased from Edwic. NaOH pellets obtained from Cambrian Chemicals Inc. Egyptian Olive pomace from South Sinia, dried, milled and sieved to get 75 μm size fractions. For all experiments, double distilled water used. Stock solution (500 mg/L) of Cu(II) prepared by dissolving 0.9505 g of cupric nitrate $[Cu(NO_3)_23H_2O]$ in 500 mL of double distilled water and 500 mg/L for Ni(II) prepared by dissolving 1.683 g of ammonium nickel(II) sulfate $[(NH_4)_2SO_4NiSO_46H_2O]$ in 500 mL of double-distilled water. The 0.1 M NaOH and 0.1 M HCl used for pH adjustments of the test solutions.

2.2. Preparation of nanomagnesium oxide (NMO)

Nano-magnesium oxide (NMO) prepared via hydroxide precipitation from aqueous solutions followed by thermal decomposition of the hydroxide. 1 M magnesium chloride solution hydrolyzed by the addition of 2 M NaOH) (Camtakan et al., 2012). The whole solution stirred vigorously at 80 °C for 2 h. A white precipitate formed instantly indicating the formation of magnesium hydroxide. The precipitate aged in the mother liquor for 24 h. The solid phase filtrated by using a Whatman filter paper No: 44 and washed twice with deionized water and absolute alcohol methanol to remove ionic impurities, then air-dried at 60 °C for 4 h. then dried at 100 °C for 48 h. The dried powder calcined at 700 °C/2h.

$$MgCl_2 + 2NaOH \rightarrow Mg(OH)_2 + 2NaCl$$

$$Mg(OH)_2 \rightarrow MgO + H_2O$$

2.3. Preparation of nanomagnesium oxide/olive pomace (NMOOP)

3:1 Nano magnesium oxide – olive pomace composite prepared by adding 0.25 M of olive pomace to 0.75 M of $MgCl_2$. This mixture hydrolyzed at 80 °C using 2 M NaOH. After 2 h of stirring, the composite aged in the mother liquor for 24 h. A beige precipitated is formed then filtered using a Whatman filter paper No: 44 and washed twice with deionized water and absolute alcohol methanol to remove ionic impurities, air-dried at 60 °C for 4 h. then dried at 100 °C for 48 h. The dried powder calcined at 700 °C/2h. The calcined powders characterized and used for the sorption batch study.

2.4. Instruments and apparatus

Fourier transform infrared (FT-IR) spectra of the samples recorded using an IR spectrometer with Fourier transformation (Thermo Nicolet Nexus FT-IR, Waltham, MA, (USA). The scanning electron microscope combined with energy-dispersive X-ray spectroscopy and electron backscatter diffraction (SEM, FEI Quanta FEG-250, EDX). The transmission electron micrograph image, TEM, for the particle size recorded on a TEM, JEM2100, Jeol.s.b, (Japan). The X-ray diffraction (XRD) measured with a Philips X'PERT multipurpose X-ray diffract meter with copper emission lines. Thermal properties of samples studied using thermo gravimetric analysis (TGA) performed on a Perkin Elmer TGA6 instrument. The sample heated from 298 K to 973 K at a heating rate of 283 K/min under a nitrogen atmosphere with a flow rate of 20 mL/min. Particle size of the prepared samples determined using Zetasizer Nano-Zs, MALVERN (UK). Pore size distribution and corresponding porosity of the prepared powders investigated applying mercury intrusion porosimetry technique with the aid of Pore- sizer chromatech 9320 (USA).

2.5. Batch sorption studies

Batch sorption studies the sorption characteristics of the prepared samples towards binary species from aqueous solutions. It performed by variation of parameters viz. pH (1–9), metal concentrations range (50–300 mg/L) and three different temperatures to get the optimum conditions for sorption.

Sorbent and the sorbet solution were contacted in a batch-wise way and after sorption the samples separated from the solution by filtration. Metal concentrations in the test solution

measured before and after sorption by atomic absorption measurements. The removal efficiency is calculated by Eq. (1).

$$\%\ \text{Removal of Cu (II) or Ni (II) ions} = (C_0 - C_f)\ /C_o x100 \quad (1)$$

Adsorption capacity q (mg/g) calculated using Eq. (2):

$$q = C_o - C_e x\ V/m \quad (2)$$

where q is the sorption capacity of the sorbent (mg/g). C_o, C_f and C_e are the initial, final, and equilibrium concentrations of the metal ions, respectively. V is the volume of solution (L), and m is the mass of the sorbent (g) taken in.

2.6. Sorption kinetics

Kinetics models explain the progress of the sorption reaction with time. It is a means to identify the mechanism of the sorption process. The reaction in general described by the order and the rate of the reaction at which it is occurring. Pseudo-first-order kinetics, Pseudo-second-order rate kinetics, and Elovich model are applied.

2.6.1. Pseudo-first-order kinetics

The general expression of the pseudo-first-order kinetics model as proposed by Lagergren (1898) and Dakroury et al. (2020b) given in Eq. (3):

$$\text{Log}\ (q_e - q_t) = \log q_e - (k_1/2.303)t \quad (3)$$

where q_e is the amounts of metal adsorbed (mg/g) at equilibrium time and q_t is the amounts of metal adsorbed at any time t; k_1 (min^{-1}) is the first-order rate constant.

2.6.2. Pseudo-second-order kinetics

Kinetics in the form of pseudo-second-order (McKay and Ho, 1999) described by Eq. (4):

$$t/q_t = 1/(k_2 q_e^2) + (1/q_e)t \quad (4)$$

where k_2 (g/mg min) is the second-order rate constant.

2.6.3. Elovich kinetics

Elovich equation applied for chemisorptions kinetics. It evaluated for heterogeneous surfaces (Cheung et al., 2000; Teng and Hsieh, 1999) and devised as in Eq. (5):

$$q_t = ((1/\beta)\ \ln\alpha\beta\ ) + ((1/\beta)\ \ln t) \quad (5)$$

where α and β are the Elovich constants. α (mg/g min) represents adsorption rate and β expressed desorption constant (g mg^{-1}) during any experiment related to the extent of surface coverage and also to the activation energy involved in chemisorptions.

2.7. Thermodynamic studies

Thermodynamic parameters such as a change in standard free energy (ΔG^0), enthalpy (ΔH^0) and entropy (ΔS^0) for the adsorption of Cu(II) and Ni(II) ions were obtained by using Eqs. (6)–(8):

$$K_c = C_{Ae}/C_e \quad (6)$$

$$\Delta G^0 = RT\ \ln K_c \quad (7)$$

$$\ln K_c = (\Delta S^0/R) - (\Delta H^0/RT) \quad (8)$$

where K_c is the equilibrium constant at temperature T, R is the universal gas constant (8.314×10^{-3} kJ/mol K) and C_{Ae} and C_e are the equilibrium concentrations of adsorbate on the adsorbent and in the solution, respectively. Activation energy deciphers the nature of the process and can be determined through the Arrhenius equation (9):

$$\ln k = (\ln A) - (E_a/RT) \quad (9)$$

where E_a is the activation energy (kJ/mol), A is the frequency factor (min^{-1}) and T, the temperature in Kelvin.

2.8. Adsorption isotherms

Isotherms are the means of analyzing the adsorbate concentration in the solution and the amount adsorbed by a specific mass of adsorbent. Isotherms find the adsorption capacity of the adsorbent. They mainly depend upon the nature and type of the system. Experiments carried out to check the best-fit adsorption isotherm for describing the process at a fixed temperature by varying concentrations of metal ions.

2.8.1. Langmuir model

Langmuir isotherm works on the following assumptions (Langmuir, 1918):

- Applicable for monomolecular layer adsorption.
- Sites are homogeneous with an equal affinity toward adsorbate.
- Adsorption at one site does not affect the adjacent site

To find the maximum adsorption capacity for a single metal ion solution, equation (10) used:

$$1/q_e = (1/Q\ ) + (1/bQ)\ (1/C_e) \quad (10)$$

2.8.2. Freundlich model

This model applied for the heterogeneous surfaces with the aid of Eq. (11):

$$\ln q_e = (\ln K_f) + (1/n)\ln C_e \quad (11)$$

where K_f, is Freundlich constants and n, related to adsorption capacity and intensity (Dakroury et al., 2020a, 2020b).

2.8.3. Temkin model

Temkin isotherm model assumes that the adsorption heat of all molecules decreases linearly with the increase in coverage of the adsorbent surface and that adsorption is characterized by a uniform distribution of binding energies, up to maximum binding energy. Temkin isotherm is described by Eq. (12).

$$q_e = (RT/b)\ln K_T + (RT/b)C_e \quad (12)$$

where K_T is the equilibrium binding constant (L mol^{-1}) corresponding to the maximum binding energy, b related to the adsorption heat, R is the universal gas constant (8.314 J K^{-1} mol^{-1}) and T is the temperature (K).

Temkin isotherm model takes into account the effects of indirect adsorbate/adsorbate interactions on the adsorption

process; it is also assumed that the heat of adsorption of all molecules in the layer decrease linearly as a result of increased surface coverage.

3. Results and discussion

3.1. Characterization of the prepared materials

3.1.1. EDX analysis

Olive pomace consists of carbohydrates, lipids (remaining oil), phenols, and a number of inorganic compounds. S. 10 illustrates EDX for olive pomace. Carbon and oxygen are the most constituents of olive pomace. While Ca is elementary 14.5% weight %.

3.1.2. FT-IR analysis

Fig. 1a shows an olive pomace pattern. The peak at 3290 cm^{-1} corresponding to —OH group while the peaks at 2920 and 2854 cm^{-1} assigned to the asymmetric and symmetric stretching vibration of (cis) methylene group =CH, C— H group. The strong peak at 1027 cm^{-1} related to connections of strain C—OH primary alcohol and CN. The broad absorption band between 1200 and 935 cm^{-1} is attributed to the contribution of various functional groups, such as C—O, and C—O—C (N. Babakhouya et al., 2018). The peak at 459 cm^{-1} corresponds to the Si—O—Si bond. Fig. 1b represents the spectrum of the prepared NMO, the weak peak at 3421 cm^{-1} that is attributed to the OH stretching vibration in the crystal structure of Mg $(OH)_2$ as a result of absorption of moisture and the loss of external Mg (OH)—O (H) hydroxyl group by raising the temperature at 700 °C (Mohd Yusoff et al., 2017). The peak at 2663 cm^{-1} shows the bending vibration of the water molecule. Mg-OH vibration mode takes place at 988 cm^{-1}. The major peaks at 895 and 707 cm^{-1} assigned to stretching vibration mode for the Mg-O-Mg compound and confirmed the presence of MgO (Mohd Yusoff et al., 2017). Fig. 1 c shows the disappearing and/or a decrease in the intensity of some peaks due to the combustion of organic materials of olive pomace by calcination process at 700 °C. The O—H stretching vibrations shows slightly an increase in the intensity than that in NMO pattern due to physical adsorption water from the moisture of surrounding and increasing of porosity in NMOOP700 particles (as shown in Table 1) the peak at 3368.59 cm^{-1} corresponds to the O—H stretching band of (Mohd Yusoff et al., 2017). The band at 1441 cm^{-1} corresponds to the Mg—O stretching vibration mode (Alfaro et al. 2019). The peaks observed below 1100 and 890 attributed the vibration of Mg—O—Si bond. This confirmed the formation of NMOOP700 composite (Imani and Safaei, 2019).

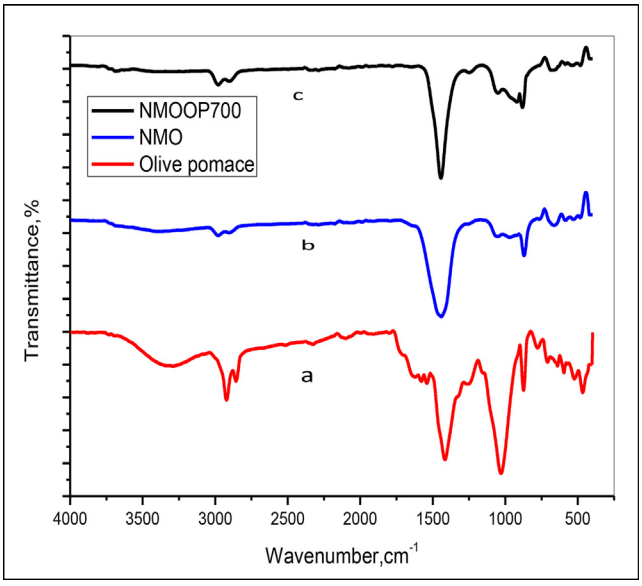

Fig. 1 FT-IR spectrum of (a) Olive Pomace, (b) NMO and (c) NMOOP700.

3.1.3. Porosity and surface characteristics

The total pore area of MgO powder increased after adding of olive pomace at calcination temperature. As the total pore area of NMO is 16.47 m^2/g and increased to more than three times 57.763 m^2/g for NMOOP700. The porosity, as well as the average pore diameter, increased. The bulk density estimate the volume of the sample plus the open and closed pores, the apparent density considers the volume of the samples and closed pores only.

Regarding the results for the NMO sample, the most pores are closed, while for NMOOP700 the open pores will increase. An expectation for the improvement of the sorption capacity for NMOOP700 is a plain fact. Specific surface area and pore size analysis with its corresponding porosity is listed in Table 1.

The particle size distribution was in nano-size for the NMO sample. After adding olive pomace, the particle size increases and the particle size distribution becomes broader. The particle size distribution is shown in Tables 2 and S.1.

3.1.4. SEM and TEM measurements

Fig. 2a shows a spherical cluster of agglomerated particles. The average size of the synthesized NMO is 50–70 nm. The agglomeration is due to the preparation technique and/or nano-character of the agglomeration particles. Fig. 3b investigates the effect of adding 25% of olive pomace where the mean particle size increases. Both NMO and NMOOP700 have a non-uniform distribution of cubic particle surfaces and highly porous structure appeared in agreement with the porosity measurement results. Fig. 2c, TEM analysis of NMO reveals the lightly agglomerated forming small particles in a narrow size distribution with a mean value of 20 nm (Alfaro et al., 2019). When Olive pomace added to NMO (Fig. 2d) and evaporates during the calcination process, the particle size increases but some particles still in nano-sized range with a mean value 50 nm with a porous structure appearance.

3.1.5. X-ray diffraction (XRD)

XRD pattern of NMO and NMOOP700 nanoparticles depicted in Fig. 3 and the peak assignments for all samples compiled in S 11 and matched with JCPDS data (JCPDS file: 79-612 for MgO and JCPDS file: 20-258 for Carbon) (Mohd Yusoff et al., 2017). A mixture of broad and sharp peaks is present. The broad peak due to OH group adsorbed from moisture and the sharp peak due to the physical change trend and phase crystallization. The presence of carbon in NMOOP700 indicates that there is still organic residual as a

Table 1 Total pore area and pore size analysis and the corresponding porosity of the samples.

Sorbent	Total pore area (m^2/g)	Average pore diameter (nm)	Bulk density (g/mL)	Apparent density (g/mL)	Porosity (%)
NMO	16.47	891	0.5546	0.6962	20.34
NMOOP700	51.3	827	0.518	1.3607	61.92

Table 2 Particle size distribution for the prepared samples.

Sample	Particle size distribution		
	Size (nm)	Mean number (%)	Nano character
NMO	50–70	75.1	93.3%
	80–100	18.2	
	> 100	6.7	
NMOOP700	< 100	22	22%
	100–200	15	
	> 200–300	14.2	
	> 300–400	15.6	
	> 500	33.2	

result of the combustion of olive pomace (Mohd Yusoff et al., 2017).

3.1.6. Thermal measurements

TGA and DTA analysis of The samples represented in Fig. 4. The weight loss for calcined NMO is 7.1% and for NMOOP700 is 10.225%. An endothermic peak at 341 °C in the DTA diagram for NMO is due to evaporation of structural water while in the thermal analysis for NMOOP700, two endothermic peaks at 97 °C and 431 °C due to evaporation of hygroscopic physically adsorbed water and combustion of the residuals organic byproducts from olive pomace and/or structural water, respectively.

3.2. Sorption study

3.2.1. The effect of pH

The pH value has a great effect on the interactions between the sorbent and the sorbet. It affects the metal ions solubility in the solution. To get the optimum pH values on the amount adsorbed (q_t) of Cu^{2+} and Ni^{2+} ions, different experiments were performed in the pH values from 1 to 9 (Fig. 5). The amount of adsorbed was found to increase with the increase of pH. This behavior may be due to the increase in the total net negative charges of surface sorbent which intensified electrostatic forces in the sorption process. Moreover with increasing pH, the total number of negative groups available for the binding of metal ions increased and therefore competition between proton, and metal ions became less pronounced (Kurniawan et al. 2006). Results showed that the NMOOP700 possessed optimum sorption capacity for both Ni (II) and Cu (II) ions at pH 5. The amount adsorbed of NMOOP700 towards Ni^{2+} and Cu^{2+} are 65.45, 93.45 mg g^{-1}, respectively compared with olive pomace towards Ni^{2+} and Cu^{2+} 22.3 and 33.2 mg g^{-1} and the amount adsorbed of NMO are 11.29, 30.22 mg g^{-1} towards Ni^{2+} and Cu^{2+} metal ions, respectively.

S2 shows copper (II) and Nickel (II) ions speciation that carried out using Hydra/Medusa chemical equilibrium software (Puigdomenech 2013) at initial metal ions concentration 100 mg/L, room temperature, and different pH values (1–12). Fig. (S2) represents At a lower pH than 8, the dominant form of nickel was Ni^{2+}; while at pH more than 8, $Ni(OH)_2$ was present as a precipitate. Whereas Cu $(OH)_2$ will be the dominant species at pH more than pH 6.

3.2.2. Effect of contact time & temperature

In order to establish the equilibrium time for maximum uptake and to determine the kinetics of the adsorption process, Cu^{2+} and Ni^{2+} sorption on NMOOP700 the sorbent was investigated as a function of contact time and the results are shown in Fig. 6. Cu(II) and Ni(II) ions were maintained for almost four hours to ensure that equilibrium was really achieved as each sample was withdrawn every five minutes' time interval. In the initial stages, the removal efficiency of the metal ion increased rapidly due to the abundant availability of active binding sites on the sorbent, and with gradual occupancy of these sites, the sorption became less efficient in the later stages. That means that the equilibrium status can be achieved after 30 min to calculate the value of q_e. This is consistent with the finding of Farhan et al. (2018).

3.2.3. Effect of ligands

The presence of ligands in anionic form also affects the sorption of Cu^{2+} and Ni^{2+} on NMOOP700 by competing the available sorption sites and/or reducing the surface char. The concentration of these ligands chosen to be the same (0.1 M EDTA and 0.1 M Citric acid), higher (0.5 M-EDTA and 0.5 M citric acid) and in excess (1 M EDTA and 1 M Citric acid). The pH was chosen the same as 5 to avoid hydroxide species. The result is shown in Fig. 7, A decrease in the sorption of both metal ions with an increase in the concentration of the two ligands obtained. This may due to the formation of Cu^{2+}- ligands and Ni^{2+}- ligands complex. The sorption of both metal ions was lower in the presence of EDTA than that of citric acid. The reason for the lower adsorption of metals in the presence of EDTA is the high complexation constant of the ligands which forms larger sizes of Metal- ligands complexes thereby hindering their introduction into the interlayer of NMOOP700 (Izquierdo et al., 2013). Furthermore, it observed that the percentage removal of Cu (II) ions became higher than that of Ni (II) ions in the presence of citric acid and EDTA; this is because Ni (II) forms larger complexes with both ligands due to higher complexation constants than Cu (II) ion (Izquierdo et al. 2013).

3.3. Sorption kinetic studies

3.3.1. Pseudo-first order

Pseudo-first-order model represented graphically S.3 Due to Table 3, it is clear that pseudo- first order model doesn't fit

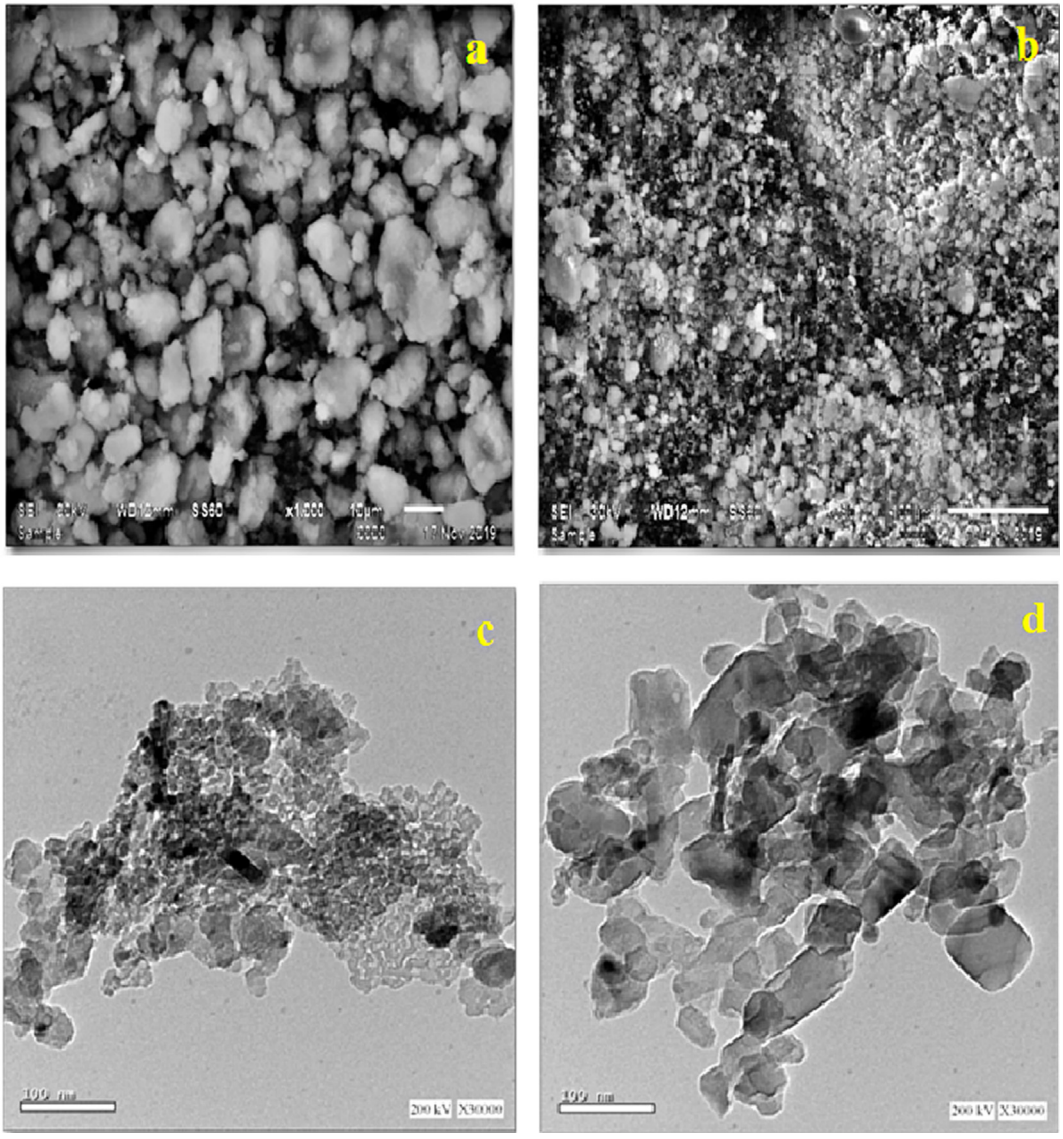

Fig. 2 SEM and TEM Analysis of (a) SEM of NMO, (b) SEM of NMOOP700, (c) TEM of NMO, and (d) TEM of NMOOP700.

with the experimental data. As the correlation coefficient (R^2) for the cations is almost low even at high temperatures. Besides, the theoretical capacity (q_e *(cal.)*) doesn't match with the experimental $q_{e(exp.)}$ for Ni^{2+} and Cu^{2+} metal ions at different temperatures.

3.3.2. Pseudo- second- order

Applying pseudo- second- order model. The fitting plots are presented in S. 4 From which it is clear that this model is more applicable to predict the sorption process mechanism, it fits with the experimental data over the range of sorption time. The calculated constants tabulated in Table 3 which shows that there is an agreement between the theoretical capacity and experimental one for the cations. Therefore, it suggests that the sorption of NMOOP700 towards Ni^{2+} and Cu^{2+} ions takes place according to pseudo-second-order kinetics and controlled by the chemo-sorption process involving valence forces through the participating or exchange of electrons between sorbent and investigated ions (Hassan and Elmaghraby, 2019). The correlation coefficients (R^2) are higher than those obtained from pseudo-first-order kinetics.

3.3.3. Elovich model

The calculated Elovich parameters (α, β) from S. 5 and the kinetic data illustrated in Table 4. The data clarify that Elovich model involves chemisorption of NMOOP700 towards Ni^{2+} and Cu^{2+} ions confirming pseudo- second- order model. It is comparable with other studied (Attallah et al., 2019).

3.4. Equilibrium isotherm studies

NMOOP700 sorption capacity estimated from the sorption isotherm models which categorized by certain constants express the affinity and surface properties of the sorbent. Moreover, they permit the calculation of NMOOP700 loading at equilibrium, which has a major impact on system economics. Initial concentration investigated for Ni^{2+} and Cu^{2+} ions solutions with various concentrations range from 50 to

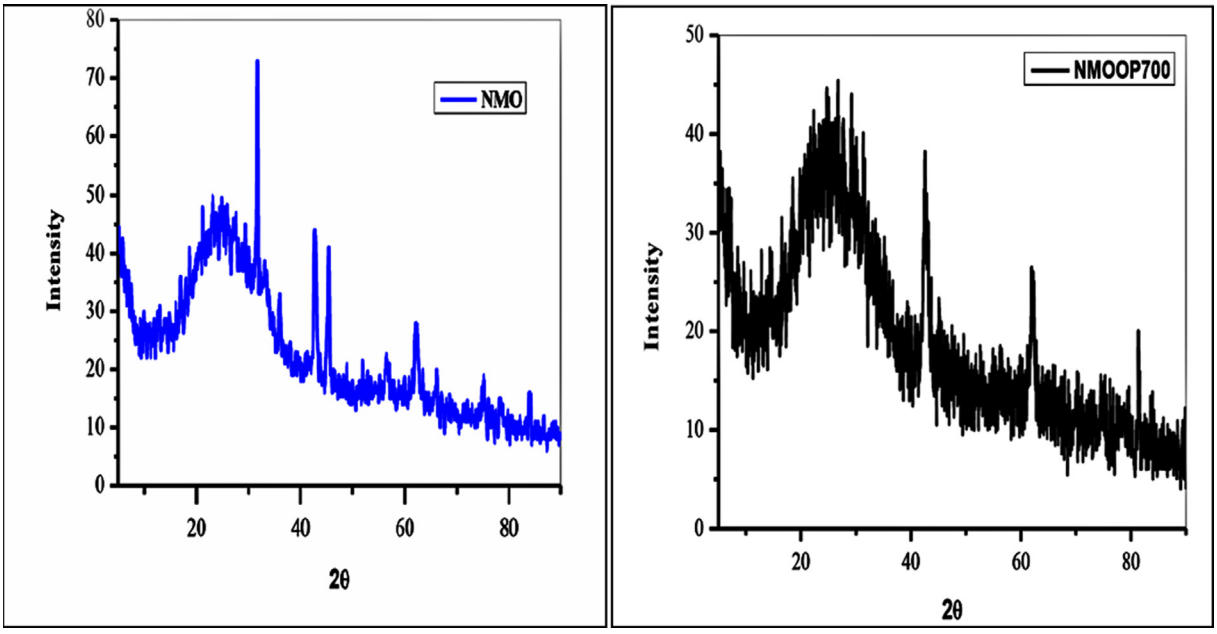

Fig. 3 XRD analysis of NMO and NMOOP700.

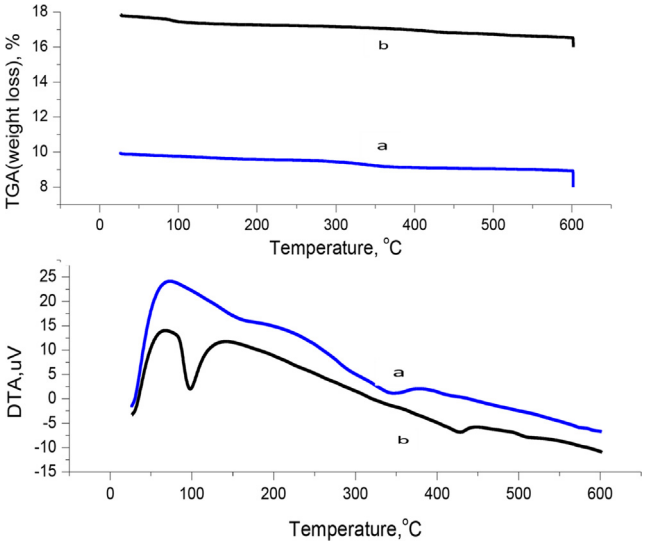

Fig. 4 TGA and DTA for the synthesized samples (a) NMO and (b) NMOOP700.

300 (mg/L); each concentration was equilibrated with 0.1 (g) NMOOP700. Fig. 8 indicates the plots between the amount of Ni^{2+} and Cu^{2+} metal ions sorbed at equilibrium q_e, onto the papered NMOOP700 and the initial metal ion concentrations C_o. From the figure, it observed that the amount sorbed of each metal ion increased with the increase of the initial concentration of the metal ions and temperature.

3.4.1. Langmuir isotherm model

S. 6 shows (C_e/q_e) versus $C_e$relation, they are straight lines for NMOOP700 towards Ni^{2+} and Cu^{2+} ions. Table 5 also reveals that Langmuir isotherm model fits well the experimental data and confirms the monolayer coverage of metal ions onto particles and also the homogenous distribution of the active sites on NMOOP700. Estimated parameters are presented in Table 5 from which, the correlation coefficients for the investigated ions were found to be (R^2) = 0.965. Moreover, the maximum monolayer capacities (Q^0) for both cations were calculated and found to be 149.9 ± 4.4 mg/g for Ni^{2+} and 186.2 ± 6.3 mg/g for Cu^{2+}. The sorption capacity of NMOOP700 towards Ni^{2+} and Cu^{2+} and the sorption energy increased with the temperature. The increase in sorption capacity with temperature attributed to the increase of the active sites on surfaces available for the sorption with increased temperature. It is obvious from Langmuir parameters in the table (4) that the process is favorable because $0 < R_L < 1$ (Dakroury et al., 2020a, 2020b).

3.4.2. Freundlich isotherm model

Plotting log q_e as a function of log C_e, carried out and represented in S. 7 for Cu^{2+} and Ni^{2+} ions. It is obvious from S. 7 that, Freundlich isotherm model doesn't fit the experimental data.

Table 5 summarizes the calculated parameters, K_f and n, which determined from the slope and the intercept of the straight lines respectively. The calculated data indicates that the value of K_f for Cu^{2+} is greater than the value for Ni^{2+} leading to a greater adsorption tendency of the NMOOP700 towards copper ions. Otherwise, the intensity constant, n values are greater than 1 indicating favorable conditions for adsorption even at high ions concentration (Ibrahim et al., 2019). Regarding to the correlation coefficient, it has smaller values, R^2 = 0.917 for Ni^{2+} and R^2 = 0.95 for Cu^{2+}, comparing to Langmuir correlation coefficient.

3.4.2.1. Temkin model. K_T and b determined from the intercept and slope of a linear relation of q_e against ln C_e (S. 8). R is Universal gas constant (8.314 J mol^{-1} K^{-1}); T is Temperature

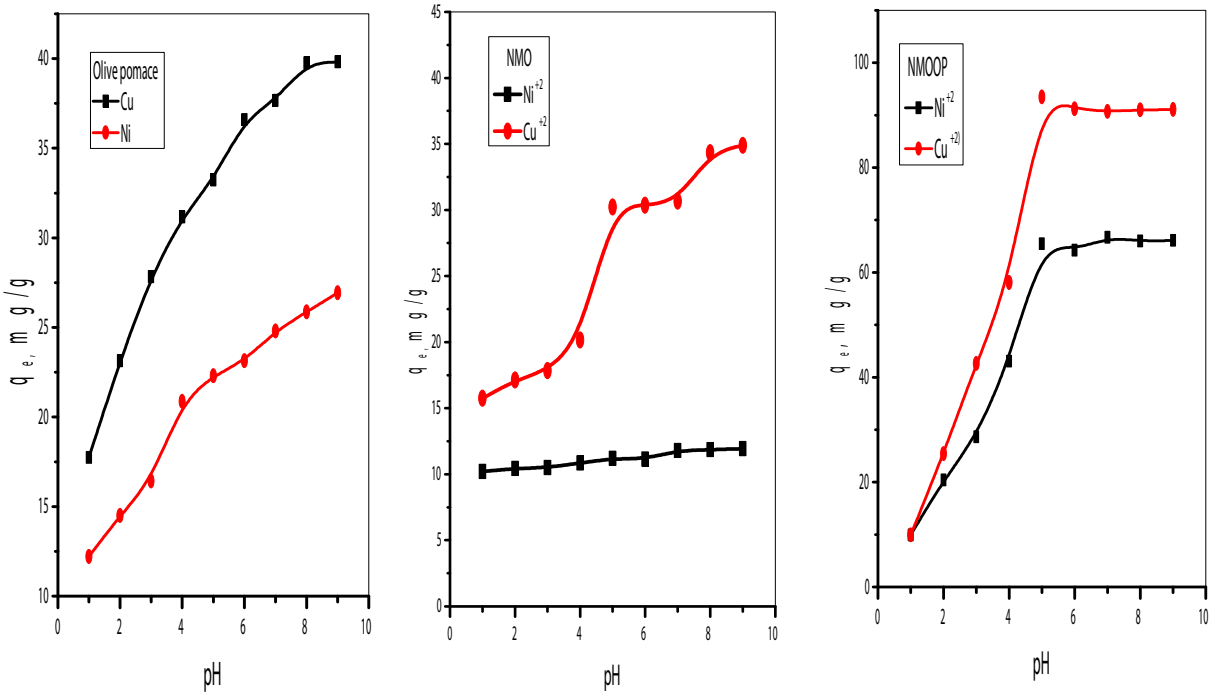

Fig. 5 Effect of pH on the amount of Cu^{2+} and Ni^{2+} adsorbed onto olive pomace, NMO, and NMOOP700.

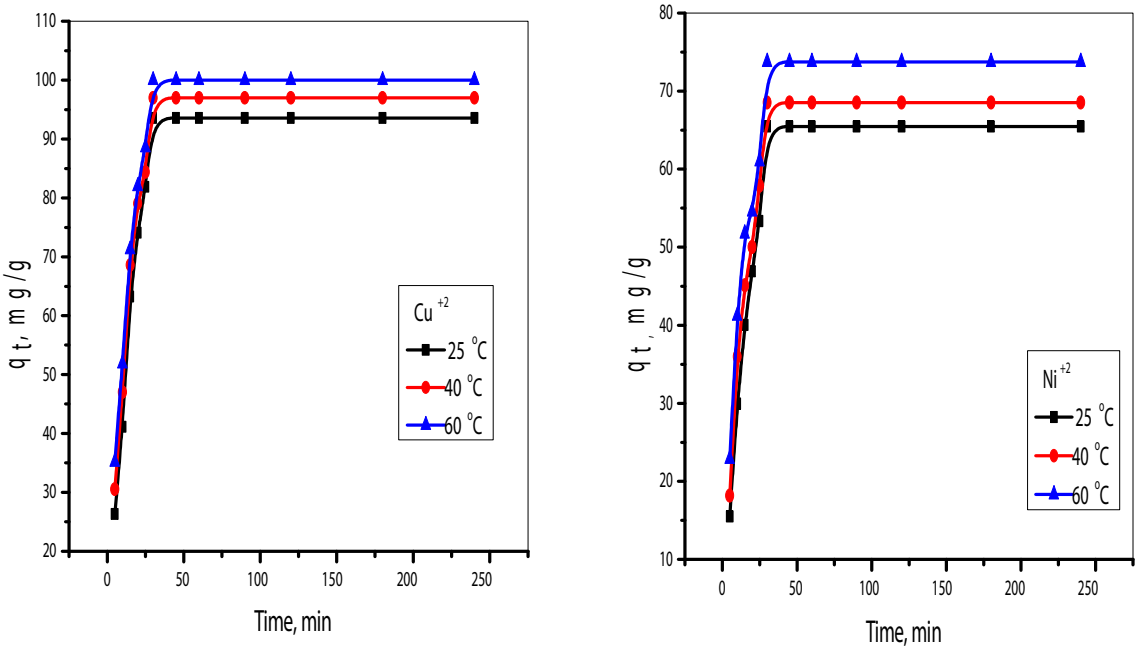

Fig. 6 Effect of contact time on the amount of Cu^{2+} and Ni^{2+} adsorbed onto NMOOP700 sample at different temperatures and pH = 5.

at 298 K. The data illustrated in Table 5. The results indicated that the Temkin constant, b, related to the heat of adsorption for the Ni^{2+} was 130.4 ± 3.2, 157.6 ± 3.6, 220.7 ± 5.5 J/mol. In the present study, the lower values of K_t indicates that the interaction between sorbent and sorbet is weak. These data supported an ion-exchange mechanism for the present work (Ghogomu et al., 2013).

3.5. Thermodynamic studies

Enthalpy change (ΔS^o) and entropy change (ΔH^o) obtained from the slope of ln (K_c) versus $(1/T)$ Graphical relation between ln (K_c) versus $(1/T)$ obtained in S. 9. Table 6 represents the calculated thermodynamics parameters for the sorption of NMOOP700 towards Ni^{2+} and Cu^{2+} metal ions;

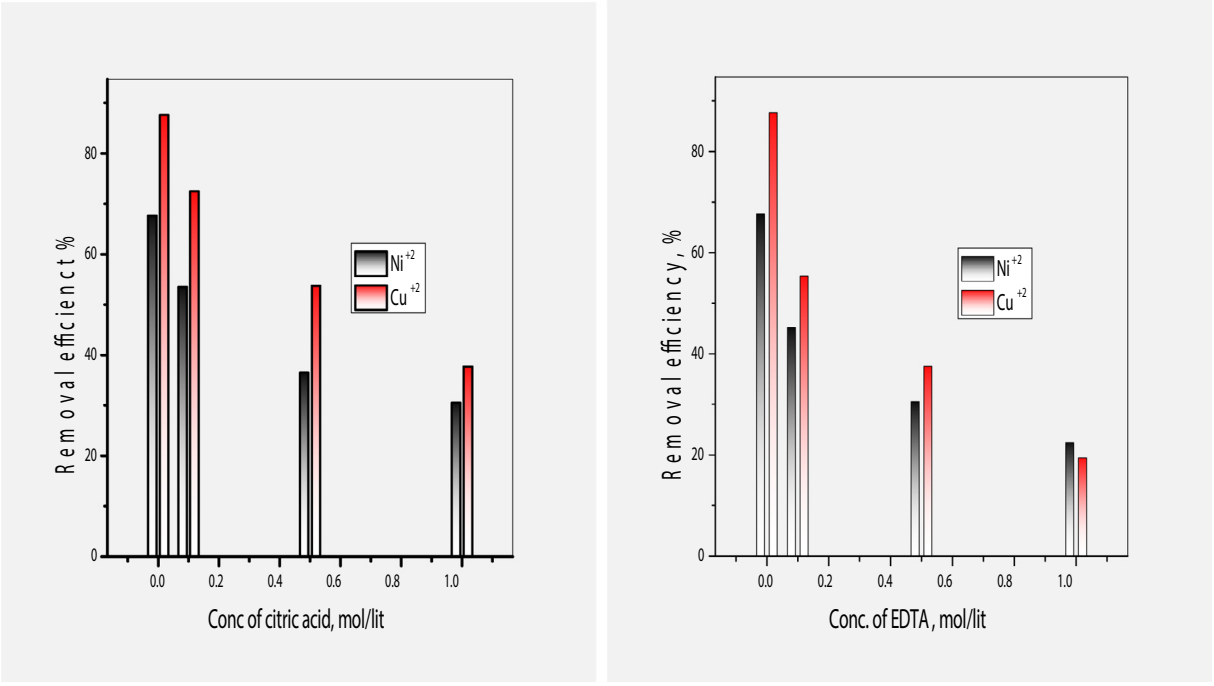

Fig. 7 Effect of ligands concentrations on the sorption of Ni^{2+} and Cu^{2+} on NMOOP700.

Table 3 Calculated parameters of the studied kinetic models for the sorption of Ni^{2+} and Cu^{2+} on NMOOP700.

Metal ion	Temp., K	First-order kinetic parameters			Second-order kinetic parameters			q_e, exp., mg/g
		k_1, min.$^{-1}$	q_e, calc., mg/g	R^2	k_2, $\times 10^{-3}$, g/mg min.	q_e, calc., mg/g	R^2	
Ni^{2+}	298	0.08 ± 0.0043	56.2 ± 2.5	0.985	1.5 ± 0.001	73.3 ± 3.2	0.999	67.7 ± 2.6
	313	0.07 ± 0.0036	56.3 ± 2.3	0.985	2.1 ± 0.01	75. 2 ± 3.3	0.999	71.1 ± 2.7
	333	0.07 ± 0.0041	53.8 ± 2.4	0.985	2.3 ± 0.002	78.5 ± 3.5	0.999	73.2 ± 2.5
Cu^{2+}	298	0.08 ± 0.0053	68.5 ± 3.1	0.979	1.9 ± 0.003	94.6 ± 5.1	0.999	87.7 ± 3.6
	318	0.09 ± 0.0062	61.1 ± 3.3	0.989	3.1 ± 0.04	95.4 ± 5.3	0.999	91.7 ± 4.1
	338	0.08 ± 0.0057	43.5 ± 3.0	0.979	4.6 ± 0.05	97.1 ± 5.2	0.999	95.1 ± 5.2

Table 4 Calculated values of α and β in the Elovich Equation for the sorption of Ni^{2+} and Cu^{2+} on NMOOP700.

Metal ion	α	β	R^2
Ni^{2+}	1.846 ± 0.021	0.0722 ± 0.0022	0.9608
	2.7522 ± 0.032	0.0740 ± 0.0013	0.956
	4.474 ± 0.052	0.0779 ± 0.0032	0.943
Cu^{2+}	3.2775 ± 0.043	0.0588 ± 0.0011	0.9775
	14.191 ± 1.43	0.0721 ± 0.0031	0.97812
	69.693 ± 4.11	0.08592 ± 0.0041	0.9742

(ΔH^o) ΔH^o positive values for Ni^{2+} and Cu^{2+} metal ions i.e the sorption processes are endothermic. The negative values of ΔG^o ΔG^o for both two ions clarify that the investigated sorption behavior is spontaneous. The small *(ΔG^o)* ΔG^o value for Ni^{2+} means that; the sorption of cesium on NMOOP700 is more spontaneously than of Cu^{2+} (Hassan et al., 2019). Also, *(ΔS^o)* values show that during the sorption process the randomness increases at the solid-solution interface.

The mechanism of any sorption process is a significant factor to understand the retention process as well as to know the characteristics of the material which help to design a new sorbent for future applications. Electrostatics interaction between the positively charged metal ion species and the negative charge on NMOOP700 composite presented by ion exchange or Si—O—Si structures (Hassan et al., 2020).

$$n\,(\text{NMOOP700}\,\text{–OH}^-) + M^{m+} \leftrightarrow (\text{NMOOP700-O})_n M^{(m-n)} + nH^+$$

$$n\,(\text{NMOOP700}\,\text{–Si—O}^-) + M^{m+} \leftrightarrow (\text{NMOOP700-Si–O}^-)_n\, M^{(m-n)}$$

where OH—, Si—O—, and M^{m+} represent the anionic groups of NMOOP700 composite surface and the metal ions species, respectively. The sorption of metal ions species Cu^{2+} and Ni^{2+} on NMOOP700 composite is maximum at pH 5, the surface charge of NMOOP700 composite is negative while the number of protons decreases. Therefore, the positively charged metal ion species of Cu^{2+} and Ni^{2+} are sorbed onto

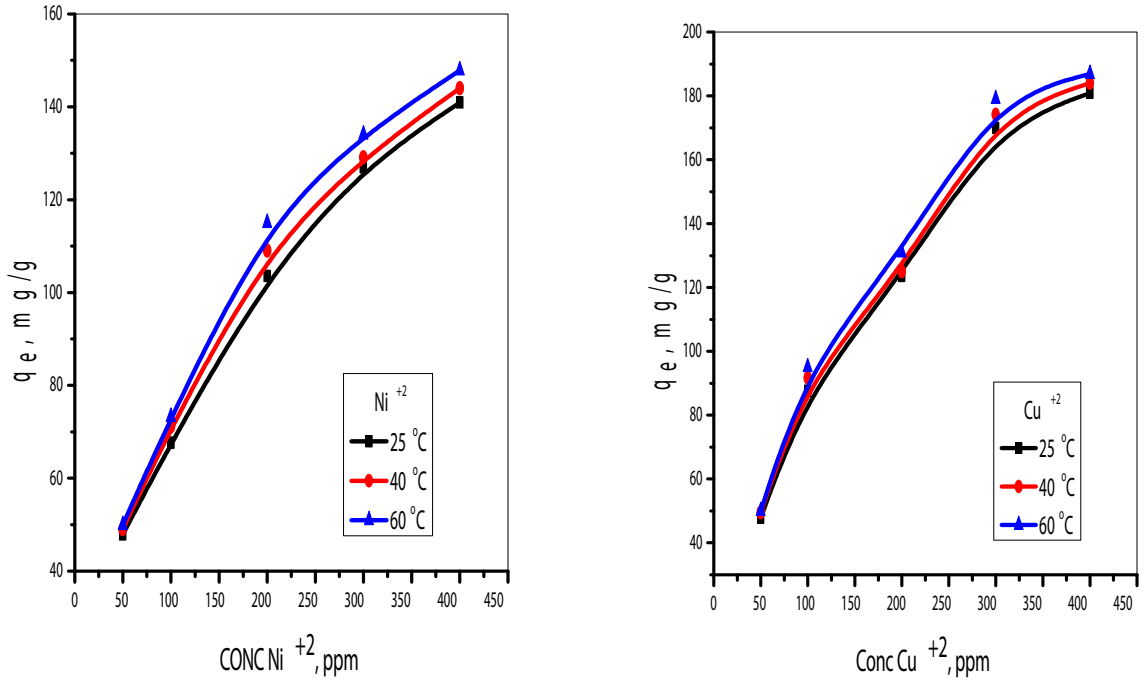

Fig. 8 Effect of metal ion concentrations on the amount sorbed of Ni^{2+} and Cu^{2+} onto NMOOP700 at different temperatures and pH = 5.

Table 5 The values of parameters of Equilibrium Isotherm models for Ni^{2+} and Cu^{2+} sorption onto NMOOP700 at pH = 5 and different temperatures.

Metal ion	Temperature (°C)	Langmuir isotherm model				Freundlich isotherm model			Temkin model		
		Q^o(mg/g)	b (L/mg)	R_L	R^2	K_F (mg/g)	n	R^2	b (J/mol)	K_T (L mol^{-1})	R^2
Ni^{2+}	25 °C	149.9 ± 4.4	0.037 ± 0.001	0.212	0.9691	37.2 ± 1.1	4.3 ± 0.06	0.917	130.4 ± 3.2	3.4 ± 0.09	0.82776
	40 °C	150.6 ± 5.1	0.045 ± 0.001	0.179	0.9758	45.4 ± 1.4	5.1 ± 0.05	0.908	157.6 ± 3.6	10.8 ± 0.11	0.81424
	60 °C	153.8 ± 4.9	0.053 ± 0.002	0.157	0.9795	50.0 ± 1.2	7.4 ± 0.06	0.651	220.7 ± 5.5	145.0 ± 1.4	0.73804
Cu^{2+}	25 °C	186.2 ± 6.3	0.071 ± 0.004	0.123	0.9634	39.8 ± 0.91	3.5 ± 0.01	0.952	86.9 ± 3.1	2.0 ± 0.008	0.93226
	40 °C	189.0 ± 6.1	0.076 ± 0.003	0.115	0.9654	57.0 ± 1.1	4.6 ± 0.03	0.959	120.4 ± 1.6	13.4 ± 0.09	0.88589
	60 °C	190.1 ± 6.4	0.106 ± 0.007	0.212	0.9744	89.7 ± 2.2	8.3 ± 0.06	0.932	231.8 ± 2.3	56.7 ± 0.91	0.78864

Table 6 Thermodynamic parameters for the sorption of Ni^{2+} and Cu^{2+} metal ions onto NMOOP700.

Metal ions Temperature	ΔG° , kJ/mol			ΔH°, kJ/mol	ΔS°, J/mol K
	298 K	313 K	333 K		
Ni^{2+}	−7.7 ± 0.08	−10.1 ± 0.9	−11.8 ± 0.9	27.3 ± 0.81	117.8 ± 2.3
Cu^{2+}	−10.5 ± 0.09	−11.9 ± 0.9	−14.0 ± 0.7	18.4 ± 0.87	97.2 ± 1.5

NMOOP700 surface via chemical ion exchange or electrostatics attraction (Hassan et al., 2020).

3.6. Comparison sorption capacity

The obtained sorption capacity of synthesized composite material has been compared with other materials as seen in Table 7. It can be concluded that the synthesized composite has a high adsorption capacity that can be used for Cu^{2+} and Ni^{2+} removal from aqueous solutions.

4. Conclusion

Nano-magnesium oxide modified by 25% olive pomace (NMOOP700) composite and MgO nanoparticle successfully synthesized and evaluated for sorption of Ni^{2+} and Cu^{2+} metal ions from liquid phase.

Table 7 Comparison of sorption properties of the NMOOP700 with other sorbents.

Sorbing material	Ni^{2+}, mg/g	Cu^{2+}, mg/g	References
Alkali-leached SiO_2	–	198.9	Sharaf and Hassan (2013)
Natural bentonite	17.20	28.88	Ghomri et al. (2013)
Chitosan-immobilized on bentonite	6.1	12.6	Futalan et al. (2012)
Sugar cane-based activated carbon	10.03	–	Taha et al. (2011)
Yellow Loess	1.65	1.23	Punrattanasin and Sariem (2015)
Zirconia-magnesia bi-metal composite	79.98	109.09	Abdel Moamen et al. (2017)
Oil palm and coconut shells-based activated carbons	3.18	–	Gonsalvesh et al. (2016)
Wood-activated carbon	–	–	Rajappaet al. (2014)
Nano-magnesium oxide modified by olive pomace	149.9	186.2	Present study

The sorption process improved using NMOOP700 composite; the equilibrium reached in a short time, after 30 min. The sorption process has endothermic nature; this indicated by the increase of amount sorbed with the increase of temperature. The sorption capacity of NMOOP700 towards Ni^{2+} and Cu^{2+} metal ions reached 149.93 ± 4.4 and 186.219 ± 6.3 mg/g, respectively at room temperature. The study demonstrates that NMOOP700 has the potential to be a good sorbent to remove Ni^{2+} and Cu^{2+} from aqueous solutions.

Declaration of Competing Interest

The authors declare that they have no known competing financial interests or personal relationships that could have appeared to influence the work reported in this paper.

Acknowledgement

Authors are thankful to Nuclear Chemistry Department, Hot Laboratories Centre, Atomic Energy Authority, Egypt for extending all necessary facilities and supports through this work.

Appendix A. Supplementary material

Supplementary data to this article can be found online at https://doi.org/10.1016/j.arabjc.2020.06.008.

References

Abdel Moamen, O.A., Hassan, H.S., El-Sherif, E.A., 2017. Binary oxide composite adsorbent for copper, nickel and zinc cations removal from aqueous solutions. Desalin. Water Treatm. 82, 219–233. https://doi.org/10.5004/dwt.2017.21015.

Abdullah, Jamal Al, Al Lafi, Abdul G., Al Masri, Wafa'a, Amin, Yusr, Alnama, Tasneem, 2016. Adsorption of cesium, cobalt, and lead onto a synthetic nano manganese oxide: behavior and mechanism. Water Air Soil Pollut. 227, 241. https://doi.org/10.1007/s11270-016-2938-4.

Acero, Juan L., Javier Benítez, F., Leal, I., Real, Francisco J., 2005. Removal of phenolic compounds in water by ultrafiltration membrane treatments. J. Environ. Sci. Health, Part A: Toxic/Hazard. Substances Environ. Eng. 40 (8), 1585–1603. https://doi.org/10.1081/ese-200060651.

Agrawal, A., Sahu, K.K., 2006. Kinetic and isotherm studies of cadmium adsorption on manganese nodule residue. J. Hazard. Mater. 137 (2), 915–924. https://doi.org/10.1016/j.jhazmat.2006.03.039.

Alfaro, Aline, León, Andrea, Guajardo-Correa, Emanuel, Reúquen, Patricia, Torres, Francisco, Mery, Mario, Segura, Rodrigo, Zapata, Paula A., Orihuela, Pedro A., 2019. MgO nanoparticles coated with polyethylene glycol as carrier for 2-Methoxyestradiol anticancer drug, PLoS One 14(8). https://doi.org/10.1371/journal.pone.0214900.

Al-Jlil, S.A., Alsewailem, F.D., 2009. Saudi Arabian clays for lead removal in wastewater. Appl. Clay Sci. 42 (3), 671–674. https://doi.org/10.1016/j.clay.2008.03.012.

Alyüz, B., Veli, S., 2009. Kinetics and equilibrium studies for the removal of nickel and zinc from aqueous solutions by ion exchange resins. J. Hazard. Mater. 167 (1–3), 482–488. https://doi.org/10.1016/j.jhazmat.2009.01.006.

Attallah, M.F., Hassan, H.S., Youssef, M.A., 2019. Synthesis and sorption potential study of Al_2O_3-ZrO_2-CeO_2 composite material for removal of some radionuclides from radioactive waste effluent. Appl. Radiat. Isotopes 147, 40–47. https://doi.org/10.1016/j.apradiso.2019.01.015.

Babakhouya, N., Abdouni, M., Louhab, K., 2018. Preparation and characterization study of an olive pomace - polyaniline composite conductor in the recovery of heavy metals by electrosorption and adsorption. J. Environ. Sci. Technol. 4 (2). ISSN : 2437-1114.

Caetano, M., Valderrama, C., Farran, A., Cortina, J.L., 2009. Phenol removal from aqueous solution by adsorption and ion exchange mechanisms onto polymeric resins. J. Colloid Interface Sci. 338 (2), 402–409. https://doi.org/10.1016/j.jcis.2009.06.062.

Camtakan, Z., Erenturk, S., Yusan, S., 2012. Magnesium oxide nanoparticles: preparation, characterization, and uranium sorption properties. Environ. Progr. Sustain. Energy 31, 536–543. https://doi.org/10.1002/ep.10575.

Caston, J.A., Fuller, C.C., Davis, J.A., 1995. Pb^{2+} and Zn^{2+} adsorption by a natural aluminum-bearing and iron-bearing surface coating on an aquifer sand. Geochim. Cosmochim. Acta 59 (17), 3535–3547. https://doi.org/10.1016/0016-7037(95)00231-N.

Cheung, C.W., Porter. J.F., Mckay, G., 2000. Sorption kinetics for the removal of copper and zinc from effluents using bone char. Sep. Purif. Technol. 19(1–2), 55–64. http://hdl.handle.net/1783.1/24689.

Dakroury, G.A., Abo-Zahra, Sh.F., Hassan, H.S., Fathy, Nady A., 2020a. Utilization of silica-chitosan nanocomposite for removal of $^{152+154}$Eu radionuclide from aqueous solutions. J. Radioanal. Nucl. Chem. 322 (3). https://doi.org/10.1007/s10967-019-06951-6. ISSN 0236-5731.

Dakroury, G.A., Abo-Zahra, Sh.F., Hassan, H.S., Elsayed Ahmed Ali, H., 2020b. Improvement of the sorption behavior of aluminum silicate composite toward 134Cs and 60Co radionuclides by non-living biomass of Chlorella vulgaris. Environ. Sci. Pollut. Res. 27, 21109–21125.

Demirbas, A., 2004. Combustion characteristics of different biomass fuels. Prog. Energy Combust. Sci. 30, 219–230. https://doi.org/10.1016/j.pecs.2003.10.004.

Dixit, S., Hering, J.G., 2003. Comparison of arsenic(V) and arsenic (III) sorption onto iron oxide minerals: implications for arsenic mobility. Environ. Sci. Technol. 15 37 (18), 4182–4189. https://doi.org/10.1021/es030309t.

El-Sayed, M.A., 2001. Some interesting properties of metals confined in time and nanometer space of different shapes. Acc. Chem. Res. 34 (4), 257–264. https://doi.org/10.1021/ar960016n.

Farhan, Salah N., Khadom, Anees Abdullah, Karim, Abdul Mun'em Abbas, 2018. Copper and lead ions removal from aqueous solution

using MgO, nanostractured MgO. Appl. Chem. Eng. 1. https://doi.org/10.24294/ace.v1i4.655.

Futalan, C., Sai, T., Lin, S., Dalida, M., Wan, M., 2012. Copper, nickel and lead adsorption from aqueous solution using chitosan-immobilized on bentonite in a ternary system. Sustain. Environ. Res. 22, 345–355.

Garg, U.K., Kaur, M.P., Garg, V.K., Sud, D., 2008. Removal of Nickel(II) from aqueous solution by adsorption on agricultural waste biomass using a response surface methodological approach. Bioresour. Technol. 99 (5), 1325–1331. https://doi.org/10.1016/j.biortech.2007.02.011.

Ghogomu, J.N., Noufame, T.D., Ketcha, M.J., Ndi, N.J., 2013. Removal of Pb(II) ions from aqueous solutions by kaolinite and metakaolinite materials. British J. Appl. Sci. Technol. 3(4), 942–961. https://doi.org/10.9734/BJAST/2013/4384.

Ghomri, F., Lahsini, A., Laajeb, A., Addaou, A., 2013. The removal of heavy metal ions (copper, zinc, nickel and cobalt) by natural bentonite. Larhyss J. 35, 37–54.

Gonsalvesh, L., Marinov, S.P., Gryglewicz, G., Carleer, R., Yperman, J., 2016. Preparation, characterization and application of polystyrene based activated carbons for Ni(II) removal from aqueous solution. Fuel Process Technol. 149, 75–85.

González-Muñoz, M.J., Rodríguez, M.A., Luquea, S., Álvareza, J.R., 2006. Recovery of heavy metals from metal industry wastewaters by chemical precipitation and nanofiltration. Desalination 200, 742–744. https://doi.org/10.1016/j.desal.2006.03.498.

Haldorai, Y., Shim, J.-J., 2014. An efficient removal of methyl orange dye from aqueous solution by adsorption onto chitosan/MgO composite: a novel reusable adsorbent. Appl. Surf. Sci. 292, 447–453. https://doi.org/10.1016/j.apsusc.2013.11.158.

Hang, C., Li, Q., Gao, S., Shang, J.K., 2012. As (III) and As (V) adsorption by hydrous zirconium oxide nanoparticles synthesized by a hydrothermal process followed with heat treatment. Ind. Eng. Chem. Res. 51 (1), 353–361. https://doi.org/10.1021/ie202260g.

Hassan, H.S., Madcour, W.E., Elmaghraby, Elsayed K., 2019. Removal of radioactive cesium and europium from aqueous solutions using activated Al_2O_3 prepared by solution combustion. Mater. Chem. Phys. 234, 55–66.

Hassan, H.S., Abdel Maksoud, M.I.A., Attia, Lamis A., 2020. Assessment of zinc ferrite nanocrystals for removal of ^{134}Cs and $^{152+154}Eu$ radionuclides from nitric acid solution. J. Mater. Sci.: Mater. Electron. 31, 1616–1633. https://doi.org/10.1007/s10854-019-02678-y.

Hassan, H.S., Elmaghraby, Elsayed K., 2019. Retention behavior of cesium radioisotope on poly (acrylamido-sulfonic acid) synthesized by chain polymerization. Appl. Radiat. isotopes 146, 40–47. https://doi.org/10.1016/j.apradiso.2019.01.017.

Henglein, A., 1989. Small-particle research - physicochemical properties of extremely small colloidal metal and semiconductor particles. Chem. Rev. 89(8), 1861–1873 https://doi.org/10.1021/cr00098a010.

Hima, K.A., Srinivasa, R.R., Vijaya, S.S., Suryanarayana, S.B., Venkateshwar, V., 2007. Biosorption: An eco-friendly alternative for heavy metal removal. Afr J Biotechnol 6 (25), 2924–2931. https://doi.org/10.5897/AJB2007.000-2461. ISSN 1684–5315.

Hristovski, K.D., Westerhoff, P.K., Crittenden, J.C., Olson, L.W., 2008. Arsenate removal by nanostructured ZrO2 spheres. Environ. Sci. Technol. 15 42 (10), 3786–3790. https://doi.org/10.1021/es702952p.

Hua, M., Zhang, S., Pan, B., Zhang, W., Lv, L., Zhang, Q., 2012. Heavy metal removal from water/wastewater by nanosized metal oxides: a review. J. Hazard. Mater. 211–212, 317–331. https://doi.org/10.1016/j.jhazmat.2011.10.016.

Ibrahim, H.A., Hassan, H.S., Mekhamer, H.S., Kenawy, S.H., 2019. Diffusion and sorption of Cs^+ and Sr^{2+} ions onto synthetic mullite powder. J. Radioanalytical Nucl. Chem. 319, 1–12. https://doi.org/10.1007/s10967-018-6322-2.

Imani, Mohammad Moslem, Safaei, Mohsen, 2019. Optimized synthesis of magnesium oxide nanoparticles as bactericidal agents. J. Nanotechnol. Article ID 6063832, 6 pages. https://doi.org/10.1155/2019/6063832.

Izquierdo, Marta, Marzal, Paula, Lens, P.N.L., 2013. Effect of organic ligands on copper(II) removal from metal plating wastewater by orange peel-based biosorbents. Water Air Soil Pollut. 224(4) https://doi.org/10.1007/s11270-013-1507-3.

Jegadeesan, Gautham, Al-Abed, Souhail R., Sundaram, Vijayakumar, Choi, Hyeok, Scheckel, Kirk G., Dionysiou, Dionysios D., 2010. Arsenic sorption on TiO_2 nanoparticles: size and crystallinity effects. Water Res. 44 (3), 965–973. https://doi.org/10.1016/j.watres.2009.10.047.

Kang, S.Y., Lee, J.U., Moon, S.H., Kim, K.W., 2004. Competitive adsorption characteristics of Co^{2+}, Ni^{2+}, and Cr^{3+} by IRN-77 cation exchange resin in synthesized Wastewater. Chemosphere 56 (2), 141–147. https://doi.org/10.1016/j.chemosphere.2004.02.004.

Kour, Jagjit, Homagai, Puspa Lal, Cagnin, Massimo, Masi, Antonio, Pokhrel, Megh Raj, Ghimire, Kedar Nath, 2013. Adsorption of Cd (II), Cu (II), and Zn (II) from aqueous solution onto nitrogen-functionalized Desmostachya bipinnata. Chem. J. 1–7. https://doi.org/10.1155/2013/649142.

Kurniawan, T.A., Chan, G.Y.S., Lo, W.H., Babel, S., 2006. Comparisons of low-cost adsorbents for treating wastewaters laden with heavy metals. J. Sci. Total Environ. 366 (2–3), 409–426. https://doi.org/10.1016/j.scitotenv.2005.10.001.

Labanda, J., Khaidar, M.S., Llorens, J., 2009. Feasibility study on the recovery of chromium (III) by polymer enhanced ultrafiltration. Desalination 249 (2), 577–581. https://doi.org/10.1016/j.desal.2008.06.031.

Lafferty, B.J., Ginder-Vogel, M., Sparks, D.L., 2010. Arsenite oxidation by a poorly crystalline manganese oxide 1 Stirred flow experiments. Environ. Sci. Technol. 44 (22), 8460–8466. https://doi.org/10.1021/es102013p.

Lagergren, S., 1898. About the theory of so-called adsorption of soluble substance. Kungliga Svenska Vetenskaps-Akademiens Handlingar 24, 1–39.

Landaburu-Aguirre, J., García, V., Pongrácz, E., Keiski, R.L., 2009. The removal of zinc from synthetic wastewaters by micellar-enhanced ultrafiltration: statistical design of experiments. Desalination 240 (1–3), 262–269. https://doi.org/10.1016/j.desal.2007.11.077.

Landaburu-Aguirre, J., Pongrácz, E., Perämäki, P., Keiski, R.L., 2010. Micellar enhanced ultrafiltration for the removal of cadmium and zinc: use of response surface methodology to improve understanding of process performance and optimisation. J. Hazard. Mater. 180 (1–3), 524–534. https://doi.org/10.1016/j.jhazmat.2010.04.066.

Langmuir, I., 1918. The adsorption of gases on plane surfaces of glass, mica and platinum. J. Am. Chem. Soc. 40, 9, 1361–1403. https://doi.org/10.1021/ja02242a004.

Lenoble, V., Laclautre, C., Serpaud, B., Deluchat, V., Bollinger, J.C., 2004. As(V) retention and As(III) simultaneous oxidation and removal on a MnO_2-loaded polystyrene resin. Sci. Total Environ. 326 (1–3), 197–207. https://doi.org/10.1016/j.scitotenv.2003.12.012.

Lin, T.F., Wu, J.K., 2001. Adsorption of arsenite and arsenate within activated alumina grains: equilibrium and kinetics. Water Res. 35 (8), 2049–2057. https://doi.org/10.1016/s0043-1354(00)00467-x.

Matlock, M.M., Howerton, B.S., Atwood, D.A., 2002. Chemical precipitation of heavy metals from acid mine drainage. Water Res. 36, 4757–4764. https://doi.org/10.1016/s0043-1354(02)00149-5.

McKay, G., Ho, Y.S., 1999. Pseudo-second order model for sorption processes. Process. Biochem. 34, 451–465.

Mohan, Dinesh, Pittman, Charles U. Jr., 2007. Arsenic removal from water/wastewater using adsorbents–a critical review, J. Hazard. Mater. 142(1–2), 1–53. https://doi.org/10.1016/j.jhazmat.2007.01.006.

Mohd Yusoff, Hanis, Rafit, Faridatu Akmar, Mohamad, Fatin Izwani, Hassan, Norhafiefa, Daud, Adibah Izzati, 2017. The effects of calcination temperatures in the synthesis of nanocrystalline magnesium oxide via sol-gel technique. Appl. Mech. Mater.

865, 36–42. https://doi.org/10.4028/www.scientific.net/AMM.865.36.

Patra, A.K., Dutta, A., Bhaumik, A., 2012. Self-assembled mesoporous g-Al_2O_3 spherical nanoparticles and their efficiency for the removal of arsenic from water. J. Hazard. Mater. 201–202, 170–177. https://doi.org/10.1016/j.jhazmat.2011.11.056.

Pena, M.E., Korfiatis, G.P., Patel, M., Lippincott, L., Meng, X., 2005. Adsorption of As(V) and As(III) by nanocrystalline titanium dioxide. Water Res. 39 (11), 2327–2337. https://doi.org/10.1016/j.watres.2005.04.006.

I. Puigdomenech, 2013. Make equilibrium diagrams using sophisticated algorithms (MEDUSA). Inorganic Chemistry. Royal Institute of Technology, Stockholm Sweden. http://www.kemi.kth.se/medusa. https://sites.google.com/site/chemdiagr/.

Punrattanasin, P., Sariem, P., 2015. Adsorption of copper, zinc, and nickel using loess as adsorbents. Pol. J. Environ. Stud. 24, 1259–1266.

Rajappa, K., Ramesh, V., Nandhakumar, 2014. Adsorption of nickel II) ion from aqueous solution onto ZnCl2 activated carbon prepared from Delonix regia pods (flame tree). IJCPS 3, 333–354.

Raven, Klaus P., Jain, Amita, Loeppert, Richard H., 1998. Arsenite and arsenate adsorption on ferrihydrite: kinetics, equilibrium, and adsorption envelopes. Environ. Sci. Technol. 32 (3), 344–349. https://doi.org/10.1021/es970421p.

Sharaf, G., Hassan, H.S., 2013. Removal of copper ions from aqueous solution using silica derived from rice straw: comparison with activated charcoal. Int. J. Environ. Sci. Technol. 11 (6), 1581–1590.

Swamy, N.K., Singh, P., Sarethy, P.I., 2011. Precipitation of phenols from paper industry wastewater using ferric chloride. Rasayan Chem 4 (2), 452–456. ISSN: 0974-1496.

Taha, F., Kiat, F., Shaharun, S., Ramli, A., 2011. Removal of Ni(II), Zn(II) and Pb(II) cations from single metal aqueous solution using activated carbon prepared from rice husk. Int. J. Env. Chem. Ecol. Geo. Geophy. Eng. 5, 112–123.

Teng, H., Hsieh, C.-T., 1999. Activation energy for oxygen chemisorption on carbon at low temperatures. Ind. Eng. Chem. Res. 38, 292–297.

Thanh, D.N., Singh, M., Ulbrich, P., Štěpánek, F., Strnadová, N., 2012. As(V) removal from aqueous media using a-MnO_2 nanorods-impregnated laterite composite adsorbents. Mater. Res. Bull. 47 (1), 42–50 https://www.cheric.org/research/tech/periodicals/doi.php?art_seq=1025051.

Van Benschoten, John E., Reed, Brian E., Matsumoto, Mark R., McGarvey, P.J., 1994. Metal removal by soil washing for an iron-oxide coated sandy soil. Water Environ. Res. 66(2), 168–174. www.jstor.org/stable/25164678.

Van Dang, Son, Kawasaki, Junjiro, Abella, Leonila C, Auresenia, Joseph, Habaki, Hiroaki, Kosuge, Hitoshi, 2008. Removal of arsenic from synthetic groundwater by adsorption using the combination of laterite and iron-modified activated carbon. J. Water Environ. Technol. 6 (1), 43–54. https://doi.org/10.2965/jwet.2008.43.

Vieira, M.G., Almeida Neto, A.F., Gimenes, M.L., da Silva, M.G., 2010. Removal of nickel on Bofe bentonite calcined clay in porous bed. J. Hazard. Mater. 176 (1–3), 109–118. https://doi.org/10.1016/j.jhazmat.2009.10.128.

Vu, A.-T., Jiang, S., Kim, Y.-H., Lee, C.-H., 2014. Controlling the physical properties of magnesium oxide using a calcination method in aerogel synthesis: Its application to enhanced sorption of a sulfur compound. Indust. Eng. Chem. Res. 53 (34), 13228–13235. https://doi.org/10.1021/ie5018546.

Xu, Z., Li, Q., Gao, S., Shang, J.K., 2010. As(III) removal by hydrous titanium dioxide prepared from one-step hydrolysis of aqueous TiCl(4) solution. Water Res 44 (19), 5713–5721. https://doi.org/10.1016/j.watres.2010.05.051.

Yan, M.A., Naiyun, G.A.O., Wenhai, C.H.U., Cong, L.I., 2013. Removal of phenol by powdered activated carbon adsorption. Front. Environ. Sci. Eng. 7, 158–165. https://doi.org/10.1007/s11783-012-0479-7.